Chemical Science



EDGE ARTICLE

View Article Online
View Journal | View Issue



Cite this: Chem. Sci., 2022, 13, 1933

All publication charges for this article have been paid for by the Royal Society of Chemistry

Received 13th October 2021 Accepted 3rd January 2022

DOI: 10.1039/d1sc05647f

rsc.li/chemical-science

Photocytotoxicity and photoinduced phosphine ligand exchange in a Ru(II) polypyridyl complex†

Sean J. Steinke,^a Sayak Gupta,^b Eric J. Piechota,^a Curtis E. Moore,^a Jeremy J. Kodanko^{*b} and Claudia Turro (1) **a

Two new tris-heteroleptic Ru(II) complexes with triphenylphosphine (PPh₃) coordination, *cis*-[Ru(phen)₂(PPh₃)(CH₃CN)]²⁺ (**1a**, phen = 1,10-phenanthroline) and *cis*-[Ru(biq)(phen)(PPh₃)(CH₃CN)]²⁺ (**2a**, biq = 2,2'-biquinoline), were synthesized and characterized for photochemotherapeutic applications. Upon absorption of visible light, **1a** exchanges a CH₃CN ligand for a solvent water molecule. Surprisingly, the steady-state irradiation of **2a** followed by electronic absorption and NMR spectroscopies reveals the photosubstitution of the PPh₃ ligand. Phosphine photoinduced ligand exchange with visible light from a Ru(II) polypyridyl complex has not previously been reported, and calculations reveal that it results from a *trans*-type influence in the excited state. Complexes **1a** and **2a** are not toxic against the triple negative breast cancer cell line MDA-MB-231 in the dark, but upon irradiation with blue light, the activity of both complexes increases by factors of >4.2 and 5.8, respectively. Experiments with PPh₃ alone show that the phototoxicity observed for **2a** does not arise from the released phosphine ligand, indicating the role of the photochemically generated ruthenium aqua complex on the biological activity. These complexes represent a new design motif for the selective release of PPh₃ and CH₃CN for use in photochemotherapy.

Introduction

Ruthenium(II) polypyridyl complexes exhibit useful excited state properties that have been explored in photochemotherapy (PCT), photodynamic therapy (PDT), and solar energy conversion, among other applications.¹⁻⁸ The spatiotemporal control possible with these complexes shows promise in alternative cancer therapies, circumventing systemic toxicity present in traditional cancer therapies, such as approved platinum drugs.9 Typically, PCT and PDT agents are activated by the absorption of visible light in the irradiated area, leading to the population of excited states that can produce cytotoxic ¹O₂ for PDT or induce the release of a therapeutic agent in PCT. Unlike complexes used in photochemotherapy, PDT agents rely on the presence of oxygen, which can represent a drawback in the hypoxic environments found in solid tumors, 10-12 making PCT agents an important area of research to advance photoinduced treatments.13-15

Coordination to the Ru(II) center through a Lewis basic site, such as a nitrile or pyridine functional group, have been explored as PCT agents and for dual PCT/PDT activity, since many drugs that can be photoreleased possess one of these groups able to coordinate to a transition metal center. ^{16–20} A frequent challenge, however, is the ability of other strong field ligands, such as phosphines, to undergo photoinduced dissociation. Importantly, molecules with a triphenylphosphinium group and cationic compounds with a triphenylphosphine (PPh₃) ligand have been shown to enhance cellular uptake, ^{21,22} leading to an interest in the investigation of divalent ruthenium triphenylphosphine complexes for PCT.

Phosphine ligands, such as PMe_3 (Me = methyl) and PPh_3 , have been shown to act as ancillary ligands that increase or promote the photosubstitution of other monodentate ligands in the Ru(II) coordination sphere.^{23–25} In particular, PR_3 (R=Me, Ph) ligands are generally stronger field ligands relative to Ncoordinated pyridine and acetonitrile. Strong π -backbonding to phosphine ligands has also been used to modify the electronic structure on the ruthenium center to reduce the overpotential of CO₂ reduction catalysts and to tune the absorption and emission properties.26-29 Whereas CH3CN and pyridine have been previously shown to undergo photoinduced ligand exchange in Ru(II) complexes, phosphine ligands are largely inert to photosubstitution.4,24,29-34 The design of complexes that can selectively photodissociate phosphines can enable the use of drugs with phosphine motifs in PCT,35-37 as well as the synthesis of supported catalysts patterned with selective irradiation.³⁸⁻⁴⁰

^aDepartment of Chemistry and Biochemistry, The Ohio State University, Columbus, OH, 43210, United States. E-mail: turro.1@osu.edu

^bDepartment of Chemistry, Wayne State University, Detroit, MI, 48208, United States. E-mail: jkodanko@wayne.edu

[†] Electronic supplementary information (ESI) available: ¹H and ³¹P{H} NMR spectra, electrochemical and X-ray crystallographic data, and DFT information (PDF). CCDC 2108338, 2109146, 2108340 and 2108925. For ESI and crystallographic data in CIF or other electronic format see DOI: 10.1039/d1sc05647f

In the present work, two new heteroleptic Ru(II) complexes containing one PPh3 and one CH3CN ligand, cis-[Ru(phen)₂(PPh₃)(CH₃CN)]²⁺ (1a, phen = 1,10-phenanthroline) and cis-[Ru(biq)(phen)(PPh₃)(CH₃CN)]²⁺ (2a, biq = 2,2'-biquinoline), were synthesized and characterized, and their structures are shown in Fig. 1. The electronic absorption, electrochemistry, and photochemistry of 1a and 2a were investigated and compared to those of their bis-acetonitrile analogs, cis-[Ru(phen)₂(CH₃CN)₂]²⁺ (1b) and cis-[Ru(biq)(phen)(CH₃CN)₂]²⁺ (2b). Based on the steric distortion introduced by the bulky PPh3 ligand, complexes 1a and 2a were expected to exhibit more facile CH₃CN dissociation. While 1a exhibits photoinduced CH₃CN exchange upon visible light excitation, 2a represents the first example of photoinduced exchange of a PPh3 ligand from a Ru(II) polypyridyl complex, a surprising departure from the commonly observed substitutional inertness of PPh3 ligands. Single-crystal X-ray structures of 1a, 2a, and the photoproduct of 2a following photolysis in CH₃CN and pyridine (I), were collected and calculations were performed on 1a and 2a to gain better understanding of the origin of the unusual photoreactivity. In addition, complexes 1a and 2a were evaluated for their toxicity against the triple-negative breast cancer MDA-MB-231 cell line in the dark and upon irradiation. The present findings show enhanced activity following photoinduced ligand dissociation for both complexes and that PPh3 release from 2a results in a modest increase in toxicity as compared to CH₃CN photodissociation in 1a. Importantly, both 1a and 2a exhibit significantly greater photoactivity than related complexes without PPh3 in their coordination sphere. The present work is consistent with greater cellular uptake by the PPh₃-containing complexes, laying the groundwork for the design of new photoactive complexes with enhanced activity.

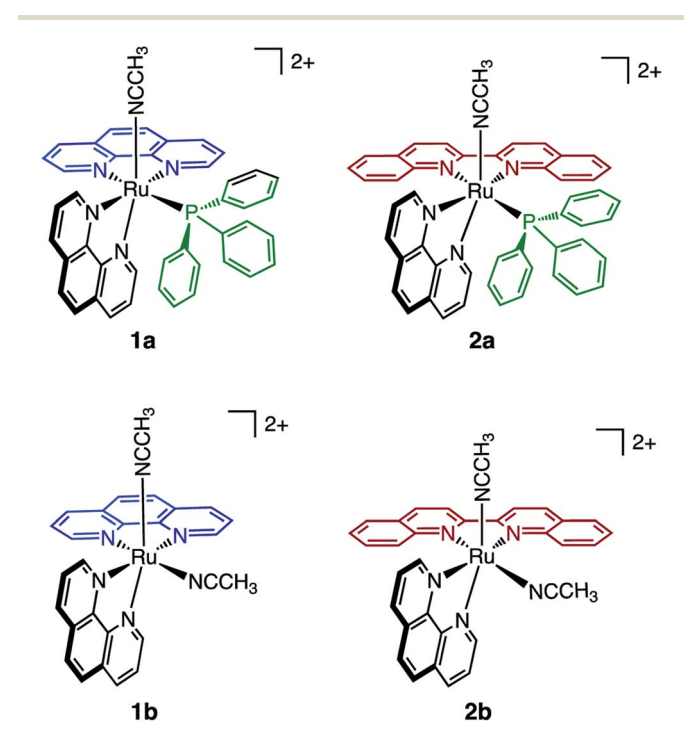


Fig. 1 Schematic representation of the molecular structures of 1a, 1b, 2a. and 2b.

Experimental

Materials

All materials were used as received without further purification, including 1,10-phenanthroline, 2,2'-biquinoline, CD₃CN, CD₃OD, (CD₃)₂CO, lithium chloride, pyridine, silver tetrafluoroborate, tetrabutylammonium hexafluorophosphate, and triphenylphosphine which were purchased from Sigma-Aldrich. Ethanol (200 proof) was obtained from Decon Laboratories, acetone, acetonitrile, dichloromethane, diethyl ether, N,Ndimethylformamide, 85% H₃PO₄, and toluene were acquired from Fischer Scientific, and ammonium hexafluorophosphate was purchased from Oakwood Chemical. Complexes 1b and 2b, ⁴¹ [Ru(phen)₂Cl₂], ⁴² [Ru(p-cymene)Cl₂]₂, ⁴³ and triphenylphosphine oxide44 were prepared according to literature procedures.

[Ru(phen)₂(PPh₃)(Cl)](PF₆)

[Ru(phen)₂Cl₂] (0.16 g, 0.30 mmol), triphenylphosphine (0.14 g, 0.53 mmol), and excess LiCl were added to 10 mL ethanol/water (1:1, v/v) mixture sparged for 15 min with N_2 . The reaction mixture was refluxed for 4 h under a nitrogen atmosphere, allowed to cool, concentrated by rotary evaporation, and then precipitated by adding it dropwise to a concentrated NH₄PF₆ solution. The product was purified by column chromatography, using a deactivated neutral alumina stationary phase and a 1:2 toluene: acetone mobile phase. The solvent was removed from the fraction containing the product via rotary evaporation, producing a dark orange solid (0.078 g, 29% yield). ¹H NMR (400 MHz, $(CD_3)_2CO$, Fig. S1†): δ 9.72 (d, 1H, J = 5.4 Hz), 8.77 (m, 2H), 8.68 (d, 1H, J = 8.2 Hz), 8.55 (dd, 1H, J = 5.7, 3.9 Hz), 8.37 (s, 2H), 8.36 (d, 1H, J = 1.3 Hz), 8.30 (d, 1H, J = 8.8), 8.23 (dd, 1H, J = 8.8)J = 20.3, 9.0 Hz), 8.13 (d, 1H, J = 8.8 Hz), 7.90 (dd, 1H, J = 8.2, 5.3 Hz), 7.86 (dd, 1H, I = 8.2, 5.3 Hz), 7.77 (dd, 2H, I = 8.3, 5.3 Hz), 7.65 (d, 1H, 5.3 Hz), 7.53 (m, 2H), 7.37 (t, 5H, J = 8.7 Hz), 7.27 (t, 2H, J = 7.6 Hz), 7.11 (m, 6H). 31 P{H} NMR (400 MHz, $(CD_3)_2CO$, Fig. S2†): δ 45.1 (s, 1P).

$[Ru(phen)_2(PPh_3)(CH_3CN)](PF_6)_2$ (1a)

[Ru(phen)₂(PPh₃)Cl](PF₆) (0.058 g, 0.064 mmol) was dissolved in 10 mL of acetonitrile/H₂O (1:1, v/v) mixture and, under an atmosphere of nitrogen, was refluxed overnight. After cooling to room temperature, the reaction solution was added dropwise to a concentrated aqueous NH₄PF₆ solution. The precipitate that formed was collected by filtering over Celite and purified on a neutral alumina column eluted with a 1:2 toluene: acetone mobile phase. The purified solution was collected and the solvent was removed via rotary evaporation, affording the desired product as a yellow-orange solid (0.031 g, 53% yield). ¹H NMR (400 MHz, CD₃CN, Fig. S3†): δ 9.41 (d, 1H, J = 5.3 Hz), 9.09 (d, 1H, J = 5.2 Hz), 8.82 (dd, 1H, J = 8.4, 1.2 Hz), 8.59 (dd, 1H, J = 6.4, 1.2 Hz)8.3, 1.2 Hz), 8.55 (dd, 1H, J = 8.2, 1.3 Hz), 8.37 (dd, 1H, J = 8.3, 1.2 Hz), 8.24 (dd, 2H, J = 28, 8.8 Hz), 8.13 (dd, 2H, J = 18, 8.8 Hz), 7.90 (dd, 1H, J = 3.0, 5.3 Hz), 7.75 (dd, 1H, J = 3.0, 5.3 Hz), 7.49 (m, 1H), 7.43 (m, 1H), 7.37 (m, 4H), 7.19 (m, 7H), 7.03 (td, 6H, J = 9.4, 1.1 Hz, 2.17 (s, 3H). ³¹P{H} NMR (400 MHz, CD₃CN,

Edge Article Chemical Science

Fig. S4†): δ 45.3 (s, 1P). ESI-MS(+): $[M-PF_6]^+$ m/z = 910.193 (calc. m/z = 910.123).

[Ru(p-cymene)(phen)Cl]

[Ru(p-cymene)Cl₂]₂ (0.30 g, 0.50 mmol) and 1,10-phenanthroline (0.19 g, 1.1 mmol) were dissolved in 4 mL acetonitrile and refluxed under a nitrogen atmosphere for 2 h, during which time a change from a red to orange solution was observed. A yellow-orange solid was collected by filtering over Celite (0.37 g, 82% yield). ¹H NMR (400 MHz, CD₃OD, Fig. S5†): δ 9.84 (d, 2H, J = 5.5 Hz), 8.84 (d, 2H, I = 8.3 Hz), 8.21 (s, 2H), 8.11 (dd, 2H, I =8.3, 5.3 Hz), 6.23 (d, 2H, J = 6.5 Hz), 6.00 (d, 2H, J = 6.2 Hz), 2.66 (q, 1H, J = 7.0 Hz), 2.27 (s, 3H), 0.99 (d, 6H, J = 6.9 Hz).

[Ru(biq)(phen)Cl₂]

[Ru(p-cymene)(phen)Cl] (0.33 g, 0.68 mmol), 2,2'-biquinoline (0.18 g, 0.69 mmol), and excess LiCl were dissolved in 2 mL N,Ndimethylformamide and refluxed under a nitrogen atmosphere for 90 min. After refluxing was complete, the reaction mixture was allowed to cool to room temperature and then added dropwise to 30 mL aqueous LiCl solution, producing a dark green solution. A dark green solid was collected via vacuum filtration and was rinsed three times each with 20 mL $\rm H_2O$ and 20 mL diethyl ether. The solid was dissolved using 1 L of a CH_2Cl_2 /methanol (1 : 1, v/v) solvent mixture, which was then removed by rotary evaporation to afford the desired product as a dark green solid (0.18 g, 44% yield).

[Ru(biq)(phen)(PPh₃)Cl](PF₆)

[Ru(biq)(phen)Cl₂] (0.048 g, 0.080 mmol), triphenylphosphine (0.039 g, 0.15 mmol), and excess LiCl were added to a 10 mL ethanol/water (1:1, v/v) mixture sparged for 15 min with N_2 . The reaction mixture was refluxed for 4 h under a nitrogen atmosphere, allowed to cool, concentrated by rotary evaporation, and then added dropwise to a concentrated NH₄PF₆ solution to produce a purple precipitate. The product was purified by column chromatography, using a neutral alumina stationary phase and an acetone mobile phase. The solvent was removed from the fraction containing the product via rotary evaporation producing a red-purple solid (0.052 g, 66% yield). ¹H NMR (400 MHz, (CD₃)₂CO, Fig. S6†): δ 10.21 (s, 1H), 8.90 (m, 4H), 8.61 (d, 2H, J = 7.8 Hz), 8.53 (d, 1H, J = 8.1 Hz), 8.30 (t, 2H, J = 8.1 Hz) = 7.3 Hz), 8.12 (d, 1H, J = 8.2 Hz), 8.06 (dd, 1H, J = 8.1, 5.5 Hz), 7.85 (dd, 3H, J = 32.8, 9.0 Hz), 7.63 (m, 3H), 7.52 (t, 1H, J = 7.6Hz), 7.28 (t, 2H, 7.5 Hz), 7.17 (s, 3H), 6.95 (m, 12H). ³¹P{H} NMR (400 MHz, $(CD_3)_2CO$, Fig. S7†): δ 42.5 (s, 1P).

[Ru(biq)(phen)(PPh₃)(CH₃CN)](PF₆)₂ (2a)

[Ru(biq)(phen)(PPh₃)Cl](PF₆) (0.044 g, 0.038 mmol) and AgBF₄ (0.019 g, 0.099 mmol) were dissolved in 10 mL of a CH₃CN/H₂O (1:1, v/v) mixture and were refluxed overnight under a N_2 atmosphere. After cooling to room temperature, the reaction mixture was added dropwise to a concentrated NH₄PF₆ solution, precipitate was collected by filtering over Celite, and then purified via bulk recrystallization using vapor diffusion of ether into a concentrated solution of 2a in acetonitrile, which afforded a red-orange solid (0.013 g, 35% yield). ¹H NMR (400 MHz, CD₃CN, Fig. S8†): δ 10.1 (d, 1H, J = 5.3 Hz), 8.96 (d, 2H, J = 8.7Hz), 8.69 (d, 2H, J = 8.8 Hz), 8.30 (m, 5H), 8.19 (m, 5H), 8.07 (dd, 5H)2H, J = 5.4, 2.8 Hz, 7.64 (m, 4H), 7.54 (m, 5H), 7.28 (td, 3H, J =7.4, 1.1 Hz), 7.21 (td, 3H, I = 7.8, 1.5 Hz), 7.16 (td, 3H, I = 7.9, 1.4 Hz), 2.34 (s, 3H). 31 P{H} NMR (400 MHz, CD₃CN, Fig. S9†): δ 42.3 (s, 1P). ESI-MS(+): $[M-PF_6]^+$ m/z = 986.252 (calc. m/z = 986.155).

Instrumentation and methods

Electronic absorption spectra were collected using a Hewlett-Packard 8454 diode array spectrophotometer in 1 cm \times 1 cm quartz cuvettes. The irradiation source for photolysis experiments was a 150 W Xe arc lamp (UHSIO) in a MilliArc lamp housing unit equipped with an LPS-220 power supply and an LPS-221 igniter (PTI). Irradiation wavelengths for quantum yield determination were selected by using bandpass and long-pass filters (CVI Melles Griot). Samples for photolysis were prepared under red light, sealed in an NMR tube (NMR) or cuvette (UV-Vis), and purged with N2 for 15 min prior to irradiation.

The ¹H and ³¹P{H} NMR spectra were obtained using a Bruker 400 MHz DPX instrument in CD₃CN, (CD₃)₂CO, or CD₃OD. ¹H chemical shifts were referenced to the residual protonated solvent peak and ³¹P{H} shifts were referenced to an external 85% H₃PO₄ standard (0 ppm). ¹H and ³¹P{H} NMR photolysis experiments were performed in CD₃CN. Electrospray ionization mass spectrometry (ESI-MS) was performed using a Bruker microTOF instrument. For ESI-MS experiments, samples were dissolved in CH3CN and referenced to a sodium trifluoroacetate standard.

Electrochemistry experiments were performed on a BASi model CV-50 W voltammetric analyzer (Bioanalytical Systems, Inc.) with a three-electrode cell utilizing a glassy carbon working electrode, a Pt wire auxiliary electrode, and a saturated Ag/AgCl (3 M NaCl) reference electrode. Samples were dissolved in acetonitrile containing 0.1 M tetrabutylammonium hexafluorophosphate (TBAPF₆) as an electrolyte, data was collected at a scan rate of 200 mV $\rm s^{-1}$, and ferrocene was added at the end of each experiment as an internal reference (+0.43 V vs. Ag/AgCl in acetonitrile).45

Crystals suitable for X-ray diffraction were obtained through vapor diffusion of diethyl ether into concentrated acetonitrile or pyridine solutions of the desired complex. Single crystal X-ray diffraction for 2a was performed using a dark red rectangular plate crystal in a nitrogen gas stream at 150 K. The diffraction pattern was collected using a Nonius Kappa APEXII CCD diffractometer and Mo K_{α} radiation ($\lambda = 0.7107$ Å). Data were integrated using the Bruker SAINT software program and scaled using the SADABS software program. Structures were solved and refined with the Bruker SHELXT Software Package within APEX2 and Olex2. Other single crystal X-ray diffraction measurements were performed on a Bruker Kappa Photon II CPAD diffractometer equipped with Mo K_{α} radiation (1a and 2b, $\lambda = 0.71073$ Å) or Cu K_{α} radiation (I, $\lambda = 1.54178$ Å) using a dark red crystal (1a), orange plate (2b), or red blade (I) in a nitrogen gas stream at 100(2) K. The data were integrated using the Bruker SAINT software program and scaled using the SADABS software program. Solution by direct methods (SHELXT) produced a complete phasing model consistent with the proposed structure.

Spin restricted and unrestricted density functional theory (DFT) calculations were performed using the Gaussian09 program package.46 Geometry optimizations and vibrational frequency calculations were performed with the SDD⁴⁷ basis set on Ru and the TZVP48 basis set on all other atoms with the PBE exchange-correlation functional.49,50 The geometries of 1a, 2a, and 2b were fully optimized starting from X-ray crystal structures and were verified to have positive harmonic frequencies, confirming the calculated structures as electronic energy minima. Molecular orbital calculations utilized the hybrid functional B3LYP,51-53 with the SDD basis set on Ru and the TZVP basis set on all other atoms. Spin densities were calculated using Mulliken population analysis (MPA) methods. Molecular orbitals from the Gaussian calculations were plotted using the Chemcraft program,54 and the analysis of the molecular orbitals and Mayer bond order calculations were performed using AOMix-FO within the AOMix program. 55,56

The cell viability of all the synthesized complexes were determined by plating MDA-MB-231 cells in a 96 well plate at a density of 7000 cells per well in Dulbecco's Modified Eagle's Medium (DMEM) supplemented with 10% FBS and 1000 units per mL penicillin/streptomycin. The plates were incubated overnight in a 37 °C humidified incubator ventilated with 5% CO2. The media was aspirated off and then quadruplicate wells were treated with DMEM supplemented with 10% FBS and 1000 units per mL penicillin/streptomycin containing different concentrations (30 µM to 500 nM) of the synthesized complexes in 1% DMSO. Plates containing wells with no cells were designated as blank wells whereas wells with cells that were not treated with the compound but only DMEM supplemented with 10% FBS and 1000 units per mL penicillin/streptomycin containing 1% DMSO (vehicle) were designated as control wells. The plates were then again incubated in a 37 °C humidified incubator ventilated with 5% CO2. After 1 h of incubation, the cells were either irradiated with blue light ($t_{irr} = 20 \text{ min}$, $\lambda_{irr} =$ 460-470 nm, 56 J cm⁻²) or kept in the dark. After 20 minutes, the plates were placed in a 37 °C humidified incubator with 5% CO₂ for 72 h, after which time, 10 μL of 3-(4,5-dimethylthiazol-2yl)diphenyl tetrazolium bromide (MTT) reagent (5 mg mL⁻¹ in PBS) was added to each well of the 96 well plate and incubated in a 37 °C humidified incubator ventilated with 5% CO₂ for 2 h. The media was then aspirated off and 100 μL of DMSO was added. The plates were then shaken for 20 min to ensure complete dissolution of the purple formazan crystals formed. Absorbance of each well was then measured at 570 nm. The mean absorbance values of the blank wells were calculated and subtracted from absorbance values for each well treated with a certain concentration of a compound. The absorbance of the control wells was also taken and subtracted with the average of the blank wells. The mean of these corrected control absorbances were then calculated. Viability of the cells was finally determined by dividing the corrected absorbance of the compound wells by the mean corrected absorbance of the control wells and expressing the mean of the ratio as a percentage value. The % viability was plotted against the log of concentration (in molarity) of the compounds and the antilog of the concentration value at 50% viability was used to determine the EC_{50} value of each complex against MDA-MB-231 cells.

Results and discussion

Electronic absorption and electrochemistry

The electronic absorption spectra of 1a, 1b, 2a, and 2b are shown in Fig. 2 and the corresponding absorption maxima and extinction coefficients are listed in Table 1. The singlet metal-toligand charge transfer (1MLCT) absorption maxima of 1a in CH₃CN, attributed to Ru($d\pi$) \rightarrow phen(π *) transitions, are observed at 372 nm and 411 nm. For 2a the $Ru(d\pi) \rightarrow phen(\pi^*)$ and $Ru(\pi p) \rightarrow biq(\pi^*)$ MLCT bands are observed at 407 nm and 477 nm, respectively, in CH₃CN. The substitution of one of the phen ligands in 1a for big in 2a results in a bathochromic shift in the ¹MLCT absorption maximum, as expected from the increased conjugation and subsequently increased π -accepting character of the big ligand as compared to phen. A similar shift is observed in the ¹MLCT maxima of the bis-acetonitrile analogs, 1b and 2b, at 420 nm and 497 nm, respectively. In addition, the lower energy of the ¹MLCT transitions in 1b and 2b, as compared to the corresponding peaks in 1a and 2a, are consistent with the increased π -accepting character of the phosphine ligand as compared to acetonitrile.26,31,57-59

The electrochemical reduction potentials for complexes 1a and 2a obtained from cyclic voltammetry (CV) experiments are listed in Table 1 and the corresponding CVs are shown in Fig. S10,† and are compared to those previously reported for 1b and 2b.⁴¹ The first reversible reduction events of 1a and 1b are localized on one of the phen ligands, with $E_{1/2}$ values at -1.29 V and -1.34 V νs . Ag/AgCl, respectively, and compare well to those reported for related complexes.^{60,61} In contrast, the first reduction couples of 2a and 2b observed at -0.82 V and -0.86 V νs . Ag/AgCl, respectively, are centered on the biquinoline ligand in each complex, consistent with the lower energy lowest unoccupied π^* orbital in biq and similar to those measured in related complexes.^{60,62}

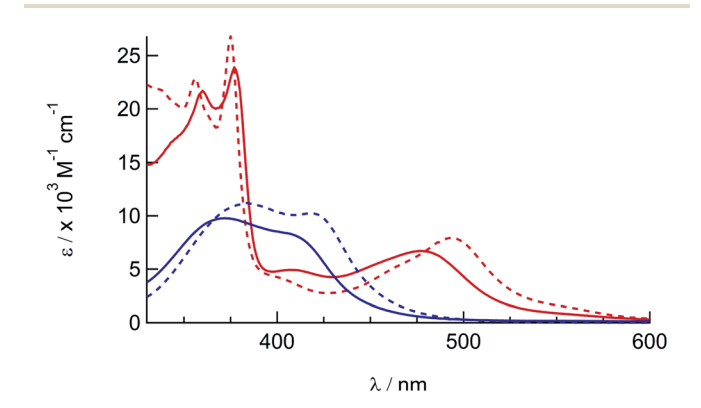


Fig. 2 Electronic absorption spectra of 1a (solid blue), 1b (dashed blue), 2a (solid red), and 2b (dashed red) in CH_3CN .

Table 1 Electronic absorption maxima (λ_{abs}), molar absorption coef-

ficients (ε), and electrochemical half-wave reduction potentials ($E_{1/2}$) in CH₃CN

Complex	$\lambda_{abs}/nm~(\epsilon/\times~10^3~M^{-1}~cm^{-1})$	$E_{1/2}/V^a$
1a	372 (9.1), 411 (7.4)	+1.62, -1.29, -1.51
$\mathbf{1b}^b$	383 (11.2), 420 (10.2)	+1.50, -1.34, -1.50
2a	360 (18), 377 (20), 407 (4.2), 477 (5.7)	$+1.67, -0.82, -1.36^{c}$
$2\mathbf{b}^b$	356 (23), 375 (27), 406 (3.9), 497 (7.8)	+1.55, -0.86, -1.40

^a 0.1 M TBAPF₆, vs. Ag/AgCl in CH₃CN. ^b From ref. 41. ^c Irreversible.

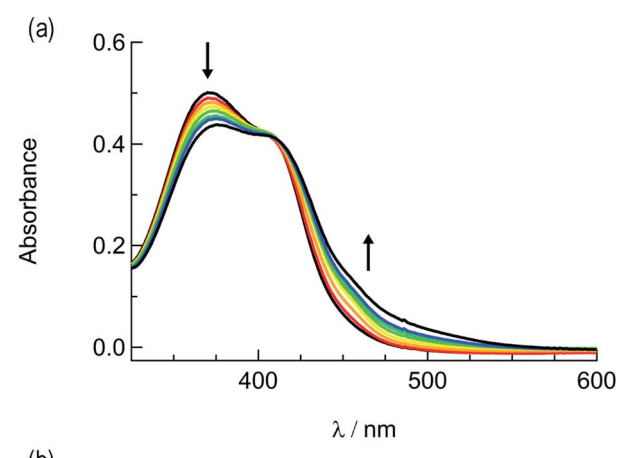
The second reduction wave is localized on the phen ligand in 2a and 2b, observed at -1.36 V and -1.40 V vs. Ag/AgCl, respectively, and on the remaining phen ligand in 1a and 1b, at -1.51 V and -1.50 V vs. Ag/AgCl, respectively. The reversible oxidation events ranging from +1.50 to +1.67 V vs. Ag/AgCl are assigned to the Ru^{III/II} redox couple (Fig. S10† and Table 1). The \sim 120 mV shift of the Ru^{III/II} couples to more positive potentials in 1a and 2a relative to those in 1b and 2b, respectively, is consistent with the greater π-accepting character of triphenylphosphine, stabilizing the highest occupied molecular orbital (HOMO). Taken together, the electrochemical data indicate that the synthetic substitution of PPh3 in 1a and 2a for CH3CN in 1b and **2b** primarily affects the energy of the $Ru(d\pi) t_{2g}$ -type orbitals.

Photochemistry

Edge Article

In order to explore the light-induced ligand dissociation in complexes 1a and 2a, their photoreactivity was investigated by monitoring changes in the electronic absorption and ¹H and ³¹P {H} NMR spectra as a function of irradiation time. Irradiation of 1a in water (<5% acetone) with visible light results in a decrease in intensity of the absorption peak at 372 nm and a concomitant increase in the 430-550 nm range with a shoulder at 455 nm, along with an isosbestic point at 407 nm (Fig. 3a). The presence of the isosbestic point is indicative of the reaction proceeding from the starting material to a single product. The changes to the ¹H NMR spectrum of 1a in CD₃CN were also monitored as a function of irradiation time, resulting in a decrease in the resonance at 2.17 ppm associated with CH₃CN bound to ruthenium and the concomitant appearance of a resonance at 1.96 ppm, corresponding to free CH₃CN (Fig. 3b). These data indicate that the irradiation of 1a results in the substitution of the CH₃CN ligand with a solvent molecule, in this case CD₃CN, with the absence of any additional photochemical reactions. The bathochromic shift in Fig. 3a is also consistent with this conclusion, as the photolysis of 1a in water results in the formation of cis-[Ru(phen)₂(PPh₃)(H₂O)]²⁺, where the bound CH₃CN is substituted for the weaker-field, π -donating H₂O ligand, thus raising the energy of the Ru(dp) t2g-type set and lowering the energy of the ¹MLCT transition. ^{34,63,64}

The irradiation of 2a in CH₃CN results in a decrease in the absorption at 407 nm and an increase a peak at 497 nm, with two isosbestic points at 396 nm and 478 nm (Fig. 4a). As shown in Fig. 4b, the spectrum of the photoproduct is nearly identical to that of 2b, providing evidence that the irradiation of 2a



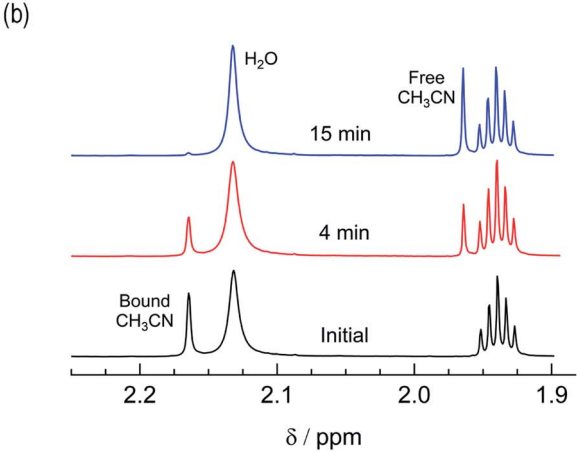
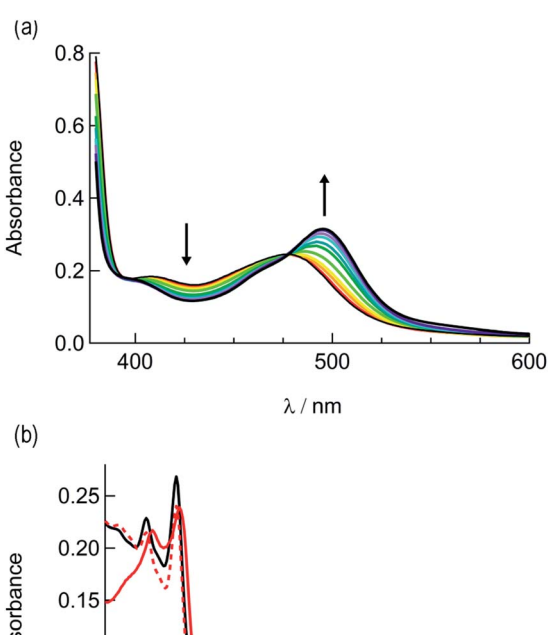


Fig. 3 Changes following the irradiation of 1a ($\lambda_{irr} \ge 395$ nm) to the (a) electronic absorption spectrum in H_2O , $t_{irr}=0-30$ min, and (b) 1H NMR spectrum in CD₃CN, $t_{irr} = 0$, 4, and 14 min.

results in the photoinduced dissociation of the PPh3 ligand generating cis-[Ru(biq)(phen)(CH₃CN)₂]²⁺, compound 2b. The changes in the ¹H NMR spectra of 2a in CD₃CN recorded as a function of irradiation time are also consistent with the exchange of the phosphine ligand following visible light irradiation (Fig. 5a). For example, the resonance at 2.34 ppm, associated with the ruthenium-bound CH₃CN ligand, decreases in intensity upon irradiation, with the concomitant growth of a peak at 2.47 ppm, associated with the photoproduct cis-[Ru(biq)(phen)(CH₃CN)(CD₃CN)]²⁺, similar to the resonances observed for the coordinated CH3CN ligands in 2b.41

The changes to the ³¹P{H} NMR spectra of 2a upon irradiation provide additional evidence for PPh3 exchange, where a decrease in intensity of the ³¹P{H} resonance at 42.3 ppm, associated with coordinated PPh3 is observed during the photolysis (Fig. 5b). Concurrently, a ³¹P{H} resonance corresponding to triphenylphosphine oxide centered at 26.0 ppm appeared as a function of irradiation time (Fig. 4d and S11†). Importantly, following 15 minutes of irradiation of 2a, the ³¹P {H} resonance associated with bound PPh3 completely disappears, while the ¹H peaks of the photoproduct cis-[Ru(biq)(phen)(CH3CN)(CD3CN)]2+ persisted. In addition, the resonance at 1.96 ppm associated with free CH₃CN appears



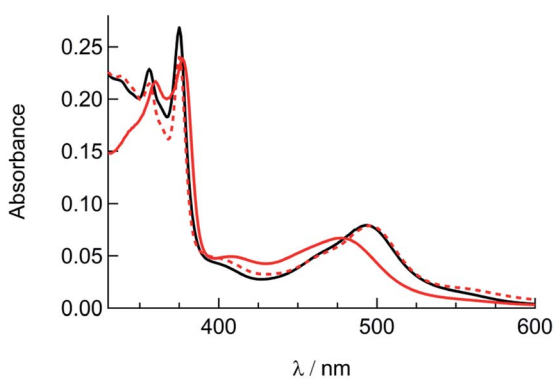
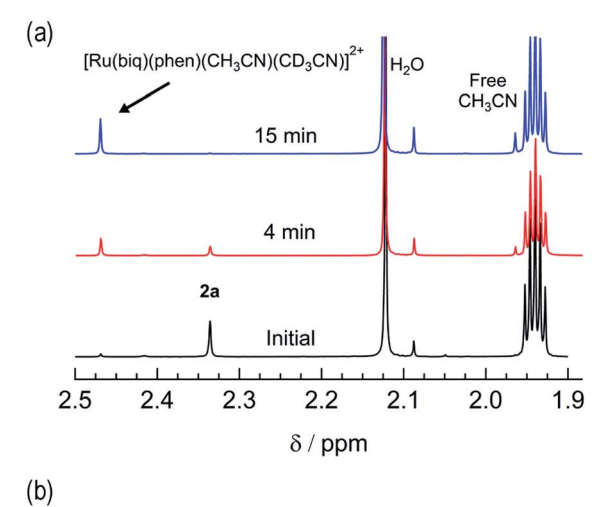


Fig. 4 (a) Changes in the electronic absorption spectrum of 2a in CH_3CN following irradiation, $t_{\rm irr}=0-5$ min and (b) electronic absorption spectra of 2a before irradiation (solid red), following 30 min irradiation (dashed red), and 2b (black).

concomitantly with the peak at 2.47 ppm, indicating CH_3CN is also photodissociated albeit not completely on the timescale of the NMR photolysis experiment.

Based on these results, the question remains whether the irradiation of 2a results in dissociation of both PPh3 and CH3CN from the starting material, or if CH₃CN exchanges only from the intermediate photoproduct cis-[Ru(biq)(phen)(CH₃CN)(CD₃CN)]²⁺ after the initial dissociation of PPh3 from the starting complex. In an effort to address this point and trap the product of the first ligand exchange step, photolysis experiments were performed in the coordinating solvent pyridine under identical illumination conditions to those previously discussed in acetonitrile, and the results are shown in Fig. 6. Inspection of Fig. 6a reveals one set of isosbestic points at early irradiation times, up to \sim 2.5 min, observed at 316 nm, 448 nm, and 500 nm, and the decrease of the peak associated with 2a at 490 nm with the appearance of a band at 540 nm. A second set of isosbestic points is evident at later times (Fig. 6b), from \sim 3.5 min to 20 min, at 338 nm, 361 nm, and 550 nm, with a loss of the species with absorption at 540 nm and the formation of the final product with maximum at 590 nm. These results point at the formation of solely one initial intermediate, I, with maximum at 540 nm, which then goes on to exchange a second ligand to generate the final product with a peak at 590 nm, assigned to cis-[Ru(biq)(phen)(py)₂]²⁺ (3). As expected from the ability of CH₃CN to π -backbond with the Ru(d π) t_{2g}-type



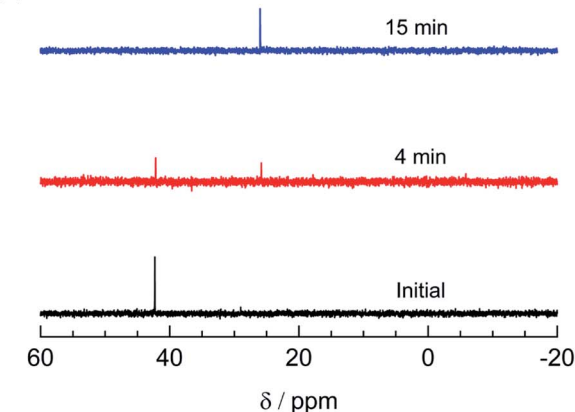


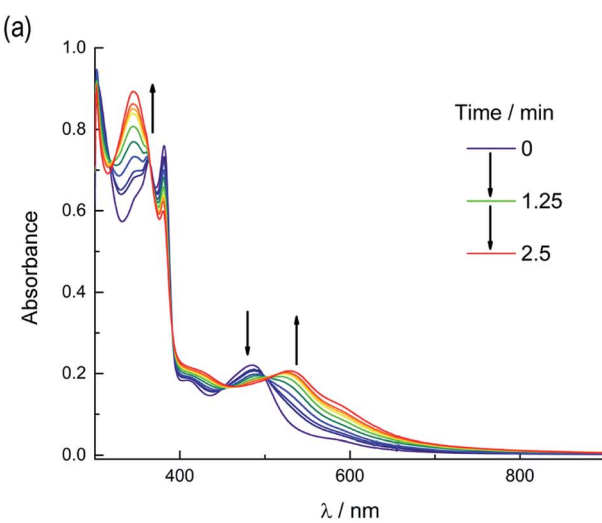
Fig. 5 Changes in the (a) 1 H and (b) 31 P{H} NMR spectra of **2a** in CD₃CN at $t_{irr} = 0$, 4, and 15 min ($\lambda_{irr} \ge 395$ nm).

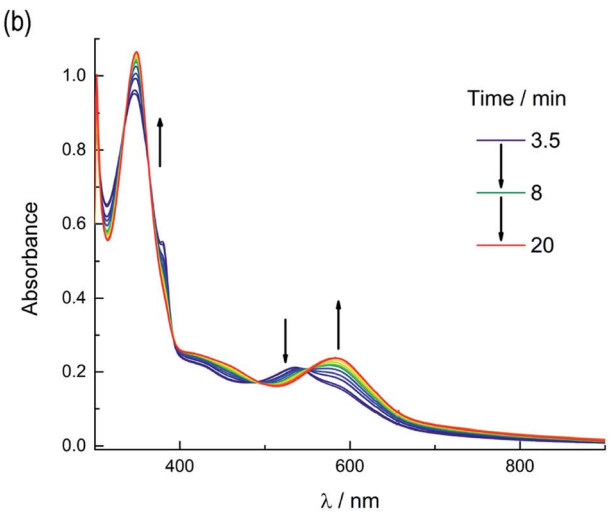
orbitals that is not present in pyridine, the ¹MLCT maximum of *cis*-[Ru(biq)(phen)(py)₂]²⁺, **3**, is red-shifted compared to that of the product **2b**, *cis*-[Ru(biq)(phen)(CH₃CN)₂]²⁺, in Fig. 4a.

intermediate The I was identified cis- $[Ru(biq)(phen)(py)(CH_3CN)]^{2+}$, generated by absorption of a single photon by 2a and photosubstitution of the triphenylphosphine ligand for a solvent pyridine molecule. Identification was supported, in conjunction with 31P{H} NMR spectra (Fig. 5b), by obtaining a single-crystal X-ray diffraction structure of the photoproduct generated by irradiating a solution of 2a in pyridine with \geq 395 nm light for 90 s (Fig. S12 and Table S1†). No further spectral changes took place after the conclusion of irradiation, indicating I is stable in the dark. This conclusion further supported by the persistence of the complex in a pyridine solution as the compound recrystallized via diethyl ether diffusion.

The presence of the two sets of isosbestic points permits determination of time-dependent concentrations of the three individual species in solution: 2a, I, and 3, during the photolysis, where I represents an intermediate species. The deconvolution of the associated spectra is possible from the known absorption spectra and molar extinction coefficients of 2a and 3, and the details of the analysis are presented in the ESI, Table

Edge Article





Changes following irradiation ($\lambda_{irr} \ge 395$ nm) in the electronic absorption spectrum of 2a in pyridine from (a) $t_{irr} = 0-2.5$ min and (b) $t_{irr} = 3.5-20 \text{ min.}$

S2, and Fig. S13.† The spectra of 2a and 3, along with that of the intermediate, I, are shown in Fig. S13,† and the time dependent mole fractions of each species were calculated over the course of the photolysis and are displayed in Fig. 7. Fig. 7 shows that the loss of 2a occurs rapidly, whereby at 70 s, 50% of the starting material remains and no amount is appreciable beyond 300 s. The formation of the intermediate I begins as early as 50 s of irradiation and reaches 99% conversion to the final product, 3, at \sim 900 s. A maximum fraction of \sim 55% of the intermediate I is apparent at \sim 150 s (Fig. 7). From the known proportions of the three species the extinction coefficient for the intermediate was estimated and compared to initial and final product values in Fig. S13.†

The PPh₃ ligand photodissociation from 2a apparent from the sequential formation of photoproducts in Fig. 6 and 7, as well as in the crystal structure of I, shows that irradiation of 2a does not result in the photodissociation of the CH₃CN ligand, such that there is no evidence of the formation of [Ru(biq)(phen)(PPh₃)(py)]²⁺ following irradiation. Instead

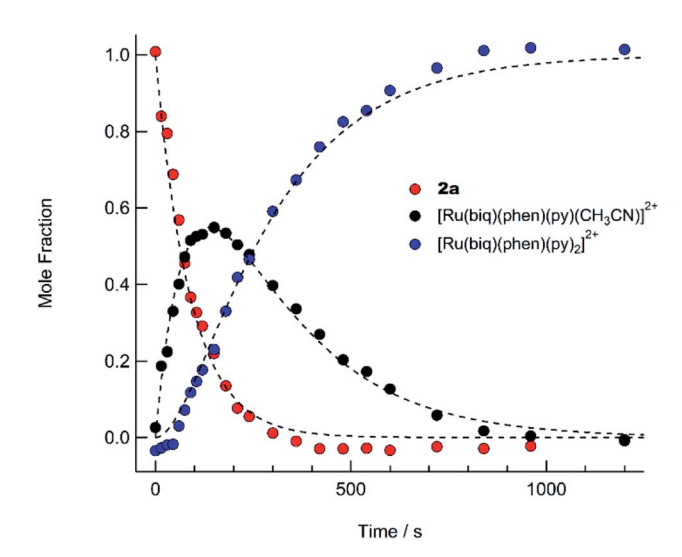


Fig. 7 Time dependent concentrations of 2a (red circles), cis- $[Ru(biq)(phen)(py)(CH₃CN)]^{2+}$ black (I, circles), $[Ru(biq)(phen)(py)_2]^{2+}$ following irradiation ($\lambda_{irr} \ge 395$ nm) in pyridine from t = 0 to t = 1200 s. The dashed lines are least-squares fits to a consecutive reaction model with a system of equations describing the time-dependent concentration of each compound (see text).

CH₃CN substitution must occur from further irradiation of the intermediate, cis-[Ru(biq)(phen)(CH₃CN)(S)]²⁺ where S = coordinating solvent molecule. It is also important to note that the growth of the ¹H NMR peak corresponding to free CH₃CN at 1.96 ppm for the irradiation of 2a in CD₃CN shown in Fig. 4c does not begin until $t \sim 4$ min, which is consistent with the dissociation of CH₃CN taking place from the intermediate cis-[Ru(biq)(phen)(CH₃CN)(CD₃CN)]²⁺ and not directly from 2a.

In contrast to the results for 2a, the 31P{H} NMR of 1a did not change as a function of irradiation time (Fig. S14†) in CD₃CN, indicating that the PPh3 ligand is photostable in this complex and does not photodissociate. Together, these results demonstrate the photoinduced ligand exchange of PPh3 from 2a upon irradiation with $\lambda_{irr} \ge 395$ nm, while **1a** undergoes only CH₃CN ligand substitution. Steric strain around the Ru(II) center due to the bulky biq ligand is known to influence the exchange of ligands from Ru(II) complexes following irradiation and likely plays a role in the photoinduced PPh3 exchange in 2a.41,65,66 The observed trends highlight a need to further investigate the geometry around the ruthenium center in phosphine complexes to identify the origin of the unusual dissociation of PPh3 in 2a.

Structural comparisons

The generally accepted model for photoinduced ligand exchange in Ru(II) polypyridyl complexes is thermal population of a ³LF (ligand field) state from a lower energy ³MLCT (metalto-ligand charge transfer) state, which places electron density on Ru-L orbital(s) with σ* anti-bonding character, leading to ligand dissociation.67-70 Distortion in the pseudo-octahedral geometry around ruthenium metal lowers the energy of the egtype σ^* set, and consequently of the dissociative ³LF state, leading to a decrease in the activation energy required to thermally populate it from the lowest energy 3MLCT state and

increasing the efficiency of ligand exchange. The introduction of steric bulk via ligands containing methyl, phenyl, or quinoline moieties has been shown to sufficiently distort the octahedral geometry, resulting in an increase the quantum yield of ligand exchange. 71-74

In order to better understand if steric effects account for the differences in the photoreactivity of 1a and 2a, their solid-state single-crystal X-ray structures were determined and are shown in Fig. 8, along with relevant bond lengths and angles listed in Table 2 with additional X-ray data available in Tables S3 and S4.† The Ru-N bond lengths from the ruthenium center to the bidentate ligand trans to the PPh3 ligand are 0.05 Å longer on average in 2a (biq) as compared to 1a (phen), respectively, indicating greater steric strain in the former. The greater steric hindrance in 2a relative to 1a is further supported by the Ru1-P1 bond length, which is 0.024 Å longer in 2a, consistent with a weaker Ru-P bonding interaction in the biquinoline complex. The crystal structure of 2b (Fig. 8), obtained by irradiating a solution of 2a in CH₃CN with visible light overnight, possesses Ru-N3 and Ru-N4 bond lengths that are 0.075 and 0.028 Å shorter than in 2a, respectively, where N3 and N4 are the nitrogen atoms in the biquinoline ligand. Such a decrease in Ru-N bond lengths demonstrates that the photodissociation of PPh3 relieves steric strain.

Evidence for distortion of the bidentate ligand *trans* to PPh₃ is apparent in the torsion angle, the angle between the two N–C–C planes formed by N3 of the bidentate ligand and the two carbon atoms bridging it to N4, expected to be 0° in an ideal octahedral geometry. In the case of 1a, the N3–C–C–N4 torsion angle in the phenanthroline ligand is $2(1)^{\circ}$. In contrast, a torsion angle of $10.5(2)^{\circ}$ is measured in the biquinoline ligand in 2a. Further, geometric planes defined by N1–Ru1–N2 and N3–Ru1–N4 would be at 90° angles in an ideal octahedral geometry and deviations from this angle reveal additional steric distortion around the metal center.⁴ The angle between these two planes in 1a was determined to be 88.69° , which is reduced to 81.37° in 2a. Importantly, in 2b this angle is 86.93° and the N3–C–C–N4 torsion angle in the biquinoline ligand is $3.1(3)^{\circ}$, showing the substitution of PPh₃ for CH₃CN allows the complex

Table 2 Selected crystallographic bond lengths and angles for 1a, 2a, and 2b

	1a	2a	2b
Bond lengths (Å)			
Ru1-N3	2.106(9)	2.148(1)	2.073(2)
Ru1-N4	2.06(1)	2.112(2)	2.084(2)
Ru1-N5	2.030(2)	2.036(2)	2.046(2)
Ru1-P1/N6	2.343(1)	2.3669(5)	2.034(2)
Torsion angles (°)			
N1-C-C-N2	1.1(4)	2.1(2)	0.6(3)
N3-C-C-N4	2(1)	10.5(2)	3.1(3)
Bond angles (°)			
N1-Ru1-N3	87.7(2)	94.09(9)	100.22(7)
N1-Ru1-P1/N6	93.68(8)	85.26(7)	82.24(7)
N2-Ru1-N3	91.2(2)	81.95(9)	87.52(6)
N3-Ru1-N5	82.1(2)	93.13(9)	93.52(7)
N4-Ru1-P1/N6	98.8(4)	103.63(7)	99.31(7)

to adopt a geometry closer to the ideal octahedral. It should be noted that the Ru–N5 bond to the CH_3CN ligand does not significantly differ in length (0.006 Å) in **1a** and **2a**.

The bond angles provided in Table 2 demonstrate additional differences in the steric distortion in **1a**, **2a**, and **2b**. For example, the N1–Ru1–N3 and N2–Ru1–N3 angles show the extent of distortion in the phenanthroline ligand in each complex. Substitution of biq for phen in **2a** pushes N1 towards the phosphine ligand while N2 moves away from P1 to accommodate the large PPh₃ unit, such that the N2–Ru1–N3 angle is nearly 10° greater in **1a** than **2a**. These same angles in **2b** demonstrate that the dissociation of PPh₃ relieves the steric strain between the polypyridyl bidentate ligands by allowing the phenanthroline ligand to move away from biq.

The angles N1-Ru1-P1 and N4-Ru1-P1 show the bulkier biquinoline ligand pushes the phosphine away from biq and toward phen in 2a, to a significantly greater extent than in the analogous phen in 1a. Similar to the bond angles, the CH₃CN ligand does not display great distortion. The only notable angle

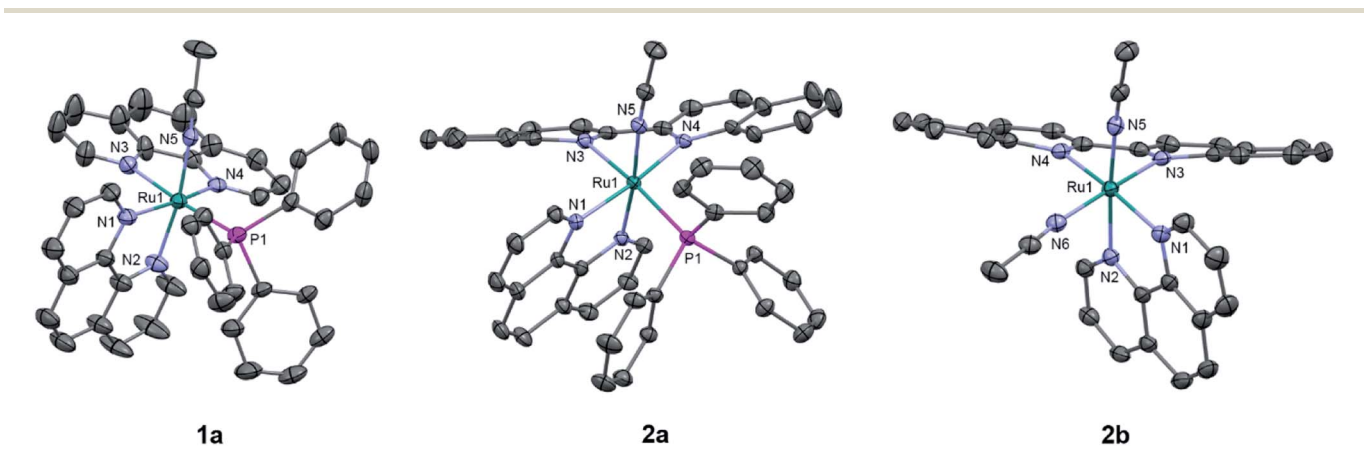


Fig. 8 ORTEP plots of 1a, 2a, and 2b (thermal ellipsoids have been drawn at 50% probability and hydrogen atoms, PF₆⁻ molecules, and co-crystallized solvent molecules have been omitted for clarity); Ru: cyan, N: light purple, C: grey, and P: magenta.

Edge Article Chemical Science

change is that for N3-Ru1-N5, which is 11° smaller in 1a than in 2a, indicating that PPh₃ pushes the acetonitrile ligand towards the trans bidentate ligand in 1a but the presence of the larger big ligand prevents this displacement in 2a. In summary, the Xray crystal structures show that there are significantly greater deviations from octahedral geometry in 2a as compared to 1a and 2b.

Calculations

Density functional theory (DFT) calculations were performed to determine if the bonding and electronic structure in the complexes could further explain the differences in the photoreactivity of 1a and 2a. Geometry optimizations in the singlet ground state (1GS) of 1a, 2a, and 2b resulted in structures in good agreement with experimental crystallographic data (Table S4). Table S4† shows that the calculated bond lengths, angles, and torsional angles are in good agreement to those obtained experimentally from the crystal structures of each complex. The ¹GS highest occupied molecular orbitals (HOMOs) in **1a** and **2a** exhibit primarily Ru-d orbital character, as is typical for Ru(II) polypyridyl complexes. 63,75-77 The lowest unoccupied molecular orbital (LUMO) in each complex is primarily localized on the ligand trans to PPh3, 1,10-phenanthroline in 1a and 2,2'-biquinoline in 2a; the latter agrees with the findings from electrochemistry (Fig. S15, S16 and Table S5†).

Geometry optimizations and vibrational frequency calculations were also performed in the triplet excited states (³ES) of 1a and 2a. In the ³ES, longer Ru-NCCH₃ and Ru-P bond distances are calculated in both complexes as compared to the corresponding ¹GS (Table 3). The calculated Ru-P bonds in the ³ES are similar, 2.475 Å in 1a and 2.473 Å in 2a, increasing from 2.411 Å and 2.441 Å in the ¹GS, respectively. However, the Ru-NCCH₃ bond is 0.04 Å longer in the ³ES of 1a, 2.055 Å, as compared to that in 2a, 2.015 Å, which may indicate that the Ru-nitrile bond is weaker in the excited state of 1a relative to that in 2a.

The differences in the bonds of 1a and 2a in the ³ES were further investigated by calculating the Mayer bond orders (MBOs) of the bonds involving ruthenium (Table 3). MBOs are an extension of Wiberg bond orders and can provide insight into the relative strengths of bonds in transition metal complexes. In the ³ES of 1a, the MBO of the Ru-NCCH₃ bond

Table 3 Selected Mayer bond orders, MBOs, and calculated bond lengths in the ¹GS and lowest ³ES of **1a** and **2a**

	MBOs			Bond Lengths/Å				
	<u>1a</u>		2a		<u>1a</u>		2a	
Bond	¹ GS	³ ES						
Ru1-N3 ^a	0.370	0.656	0.223	0.223	2.080	2.022	2.096	2.095
Ru1-N5 ^b	0.601	0.441	0.653	0.576	2.008	2.055	2.000	2.015
Ru1-N1 ^c	0.260	0.408	0.281	0.368	2.136	2.103	2.170	2.146
Ru1-P1	0.760	0.719	0.701	0.659	2.411	2.475	2.441	2.473

 $[^]a$ Bond to N atom of bidentate ligand $\it trans$ to CH_3CN. b Bond to N atom of CH₃CN. ^c Bond to N atom of bidentate ligand trans to PPh₃.

(Ru1-N5) exhibits a 26.6% decrease as compared to the ¹GS and the Ru-N(phen) bond trans to CH₃CN (Ru1-N₃) displays a dramatic 74.0% increase. These results indicate that the reduced phenanthroline ligand in the excited state exerts a trans-type influence on the CH₃CN ligand and weakens the Ru1-N3 bond, likely contributing to its dissociation in the excited state as has been observed in other Ru(II) complexes.33,78,79 In contrast, the MBO of the bond to CH3CN only decreases by 11.8% in the triplet state of 2a and the order of the Ru-N bond trans to CH3CN does not change in the triplet state of 2a. In addition, the Ru-NCCH₃ bond itself is significantly stronger in the ³ES of 2a as compared to 1a, 0.576 and 0.441, respectively.

Both 1a and 2a displayed a ~6% increase in the MBO of the Ru-PPh₃ bond, Ru1-P1 in Table 3, in the ³ES, although the bond is weaker in the excited state of 2a, MBO = 0.659, than in 1a, MOB = 0.719. The order of the bond *trans* to the phosphine ligand, Ru1-N1, is calculated to increase by 31.0% in 2a and 56.9% in 1a, indicating a trans-type influence in both complexes. However, the phenomenon is significantly stronger in 1a for the bond positioned trans to the CH₃CN ligand, Ru1-N3, which may explain why the CH₃CN ligand preferentially photodissociates in this complex.

Mulliken spin density (MSD) calculations were also performed on the lowest energy ³ES of 1a and 2a. These calculations determine the unpaired electron density on each atom in the ³ES and can provide information on the nature of the excited state. In complexes with ³LF as the lowest energy triplet excited state, the spin density on the Ru(II) metal center would theoretically equal two. If the lowest energy ³ES is MLCT in nature, the spin density on ruthenium is expected to be one, and any deviation from these whole numbers indicates metal/ ligand mixing. The MSD on ruthenium and the summed density on each ligand in the lowest energy 3ES of 1a and 2a is shown in Fig. 9. The calculated spin densities on Ru(II) indicate the lowest energy triplet excited state is MLCT in nature with notable ligand character in 1a and significant mixing from a ligand-centered state in 2a. The summed spin density on the phenanthroline ligand trans to PPh3 in 1a is 0.447, lower than the 0.763 sum on the phen ligand trans to CH₃CN, further indicating stronger trans-type influence on the nitrile ligand in the excited state. In the ³MLCT of 2a the sum of the spin density on the phen ligand, which is trans to CH₃CN, is 0.074 and a sum of 1.433 is calculated on the biquinoline ligand, indicating a significant trans-type influence on the PPh3 ligand. Taken together with the calculated bond lengths and MBOs in the ³MLCT state, it can be concluded that while **1a** exhibits a *trans*type influence on both monodentate ligands, it is stronger in the case of the CH₃CN ligand which can explain the preferential dissociation of CH₃CN upon irradiation. In the ³MLCT state of 2a there is no evidence of trans-type influence on the nitrile ligand, but a significant degree of trans-type influence is calculated for the phosphine ligand. These results, in conjunction with the steric strain evident from the crystal structure, can explain the unexpected photodissociation of the PPh₃ ligand in 2a.

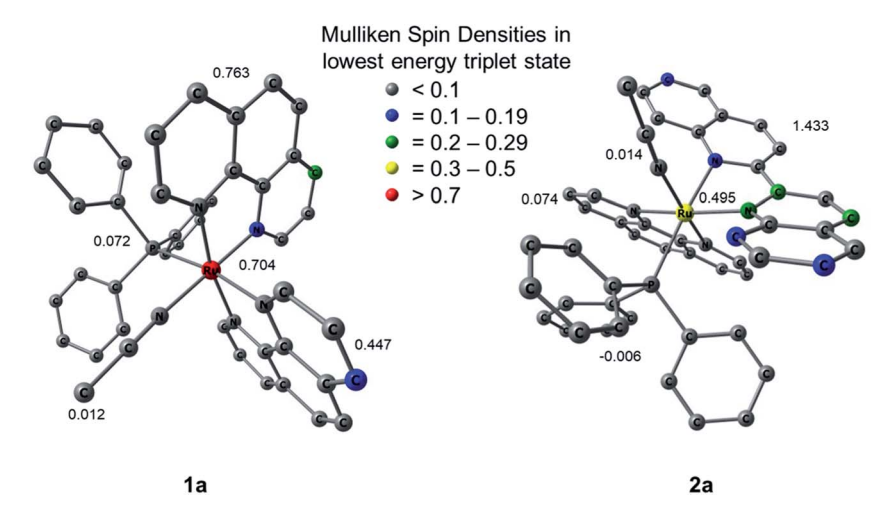


Fig. 9 Mulliken spin densities (MSDs) on ruthenium and the summed densities on each ligand in the calculated lowest energy triplet excited states of 1a and 2a.

Cell viability

The effect of photochemical reactivity on the biological behavior of 1a and 2a was investigated on the MDA-MB-231 triple-negative breast cancer cell line in the dark and upon irradiation and the results were compared to those of related complexes previously reported. 18,80,81 The half effective concentration, EC₅₀, was determined, which is defined as the concentration of the compound when the viability of the experimental cells is 50% compared to those in the absence of active compound. Complexes 1a and 2a were incubated with MDA-MB-231 cells for 1 h and were then either left in the dark or irradiated with blue light for 20 min (λ_{irr} = 460-470 nm, 56 J cm⁻²). Cellular viability was assessed using the MTT assay after 72 h, where the viability upon treatment with only the vehicle (1% DMSO) only in DMEM (Dulbecco's Modified Eagle Medium) was considered as 100%, and the results are listed in Table 3. Both 1a and 2a are non-toxic against MDA-MB-231 cells in the dark with EC_{50}^D values of 26.6 \pm 1.5 μM and >30 μM, respectively; the latter is above the maximum concentration allowed by the solubility in growth media (30 µM). However, irradiation with blue light significantly increased the toxicities of both complexes, resulting in $EC_{50}^L=4.6\pm0.6~\mu M$ for 1a and $EC_{50}^{L}=7.1\pm0.2~\mu M$ for 2a (Fig. S17 and S18†). These values of the phototherapeutic index, PI, values defined as EC₅₀/EC₅₀, were calculated to be 5.8 and >4.2 for 1a and 2a, respectively (Table 4). While complex 1a exchanges CH3CN for a solvent water molecule, 2a releases PPh3 upon irradiation. The finding that PPh3 by itself is not toxic against MDA-MB-231 cells both in the dark and when irradiated with blue light ($t_{irr} = 20 \text{ min}$, $\lambda_{irr} = 460\text{--}470 \text{ nm}$, 56 J cm⁻²) in the concentrations used for complexes 1a and 2a (Fig. S19†) led to the conclusion that the corresponding aqua complexes are the major cause of toxicity upon irradiation.

Comparison of the cell toxicity data of *cis*-[Ru(bpy)₂(PPh₃)(-CH₃CN)]²⁺ and *cis*-[Ru(bpy)₂(CH₃CN)₂]²⁺ in Table 3 indicates that the substitution of a CH₃CN ligand for PPh₃ increases the PI value of the ruthenium complex. Complexes **1a** and **2a** exhibit PI values similar to or exceeding that of *cis*-[Ru(bpy)₂(PPh₃)(-CH₃CN)]²⁺. These results indicate that the phosphine ligand

Table 4 $\rm EC_{50}$ values upon irradiation and in the dark and photochemotherapeutic index, PI, for $\rm 1a$, $\rm 2a$, and related compounds in MDA-MB-231 cancer cells

Complex	$\mathrm{EC_{50}^D}/\mu\mathrm{M}^{~a}$	$EC_{50}^L/\mu M^a$	PI^b
1a	26.6 ± 1.5	4.6 ± 0.6	5.8
2a	>30	7.1 ± 0.2	>4.2
$[Ru(bpy)_2(PPh_3)(CH_3CN)]^{2+c}$	>30	7.0 ± 1.4	>4.3
cis-[Ru(bpy) ₂ (CH ₃ CN) ₂] ^{2+ d}	244 ± 23	223 ± 94	$\textbf{1.1} \pm \textbf{0.4}$

 a Data are an average of three independent experiments. b PI = $\mathrm{EC}_{50}^\mathrm{D}$ / $\mathrm{EC}_{50}^\mathrm{L}$. From ref. 82; bpy = 2,2′-bipyridine. d From ref. 83; IC₅₀ values against HeLa cells.

may positively influence the activity against cancer cells of these ruthenium complexes, a conclusion supported by previous examples of phosphines improving cellular uptake and localizing complexes to the mitochondria, increasing selectivity for cancerous cells over healthy cells,²² and increasing cytotoxic activity against breast and colon cancer cells of phosphine containing *cis*-configured Pt(II) complexes over that of cisplatin.^{21,84-86}

Conclusion

Two new triphenylphosphine-containing complexes, 1a and 2a, were synthesized and their ground state spectroscopic and electrochemical properties were characterized, along with their photoinduced ligand exchange and cytotoxicity against a triplenegative breast cancer cell line. Changes in the electronic absorption and NMR spectra of complex 1a revealed the substitution of a CH₃CN ligand for a solvent molecule following visible light irradiation and a substitutionally inert PPh₃. In contrast, the photolysis of complex 2a results in the initial exchange of the PPh₃ ligand generating a solvated intermediate, and the latter goes on to absorb a second photon which then undergoes CH₃CN substitution. A comparison of the single crystal X-ray structures reveals that 2a exhibits greater steric

Edge Article Chemical Science

distortion around the metal center than 1a, which is subsequently relieved upon the photoinduced exchange of PPh3 for a less sterically-demanding solvent molecule. To our knowledge, this represents the first report of the photodissociation of a phosphine ligand from a Ru(II) polypyridyl complex. In addition, the ability of phosphine ligands to enhance cellular uptake was shown to enhance the photocytoxicity of 1a and 2a against a triple-negative breast cancer cell line relative to related complexes without PPh₃ in their coordination sphere. This work shows that a coordinated PPh3 ligand can serve as a new architecture for potential therapeutics for use in PCT.

Author contributions

Sean J. Steinke synthesized the complexes and conducted photophysical and photochemical measurements. Eric J. Piechota aided with data analysis and interpretation, Sayak Gupta performed the cell studies, and Curtis E. Moore collected and solved the crystal structures. Jeremy J. Kodanko and Claudia Turro advised their respective group members.

Conflicts of interest

The authors declare no competing financial interest.

Acknowledgements

The authors thank the support from the National Science Foundation (CHE-2102508), as well as Dr J. C. Gallucci for assistance with the collection of the crystal structure data of 2a.

References

- 1 N. A. Smith and P. J. Sadler, Philos. Trans. R. Soc., A, 2013, 371, 20120519.
- 2 (a) S. B. Vittardi, R. T. Magar, D. J. Breen and J. J. Rack, J. Am. Chem. Soc., 2021, 143, 526-537; (b) A. W. King, L. Wang and J. J. Rack, Acc. Chem. Res., 2015, 48, 1115-1122; (c) B. A. McClure, N. V. Mockus, D. P. Butcher, Jr, D. A. Lutterman, C. Turro, J. L. Petersen and J. J. Rack, Inorg. Chem., 2009, 48, 8084-8091.
- 3 (a) J. Karges, S. Kuang, F. Maschietto, O. Blacque, I. Ciofini, H. Chao and G. Gasser, Nat. Commun., 2020, 11, 1-13; (b) M. Jakubaszek, B. Goud, S. Ferrari and G. Gasser, Chem. Commun., 2018, 54, 13040-13059; (c) C. Mari, V. Pierroz, S. Ferrari and G. Gasser, Chem. Sci., 2015, 6, 2660-2686.
- 4 (a) J. K. White, R. H. Schmehl and C. Turro, *Inorg. Chim. Acta*, 2017, **454**, 7–20; (*b*) J. D. Knoll, B. A. Albani and C. Turro, *Acc.* Chem. Res., 2015, 48, 2280-2287; (c) J. D. Knoll and C. Turro, Coord. Chem. Rev., 2015, 282-283, 110-126; (d) Y. Sun, M. El Ojaimi, R. Hammit, R. P. Thummel and C. Turro, J. Phys. Chem. B, 2010, 114, 14664-14670.
- 5 S. Monro, K. L. Colon, H. Yin, J. Roque, P. Konda, S. Gujar, R. P. Thummel, L. Lilge, C. G. Cameron S. A. McFarland, Chem. Rev., 2019, 119, 797-828.
- 6 L. Hammarström, Acc. Chem. Res., 2015, 48, 840-850.

- 7 M. R. Gill and J. A. Thomas, Chem. Soc. Rev., 2012, 41, 3179-3192.
- 8 L. Marcelis, J. Ghesquiere, K. Garnir, A. Kirsch-De Mesmaeker and C. Moucheron, Coord. Chem. Rev., 2012, 256, 1569-1582.
- 9 R. Oun, Y. E. Moussa and N. J. Wheate, Dalton Trans., 2018, 47, 6645-6653.
- 10 R. Liu, L. Zhang, J. Zhao, Z. Luo, Y. Huang and S. Zhao, Adv. Thermoelectr., 2018, 1, 1800041.
- 11 J. Dang, H. He, D. Chen, L. Yin and L. Biomater, Sci, 2017, 5, 1500-1511.
- 12 Y. Mir, J. E. van Lier, B. Paquette and D. Houde, Photochem. Photobiol., 2008, 84, 1182-1186.
- 13 D. Havrylyuk, D. K. Heidary, Y. Sun, S. Parkin and E. C. Glazer, ACS Omega, 2020, 5, 18894-18906.
- 14 H. Shi, C. Imberti and P. J. Sadler, Inorg. Chem. Front., 2019, 6, 1623-1638.
- 15 V. H. S. van Rixel, V. Ramu, A. B. Auyeung, N. Beztsinna, D. Y. Leger, L. N. Lameijer, S. T. Hilt, S. E. Le Devedec, T. Yildiz, T. Betancourt, M. B. Gildner, T. W. Hudnall, V. Sol, B. Liagre, A. Kornienko and S. Bonnet, J. Am. Chem. Soc., 2019, 141, 18444-18454.
- 16 M. K. Herroon, R. Sharma, E. Rajagurubandara, C. Turro, J. J. Kodanko and I. Podgorski, Biol. Chem., 2016, 397, 571-582.
- 17 M. Huisman, J. K. White, V. G. Lewalski, I. Podgorski, C. Turro and J. J. Kodanko, Chem. Commun., 2016, 52, 12590-12593.
- 18 K. Arora, M. Herroon, M. H. Al-Afyouni, N. P. Toupin, T. N. Rohrabaugh, L. M. Loftus, I. Podgorski, C. Turro and J. J. Kodanko, J. Am. Chem. Soc., 2018, 140, 14367-14380.
- 19 T. N. Rohrabaugh, A. M. Rohrabaugh, J. J. Kodanko, J. K. White and C. Turro, Chem. Commun., 2018, 54, 5193-
- 20 A. Li, R. Yadav, J. K. White, M. K. Herroon, B. P. Callahan, I. Podgorski, C. Turro, E. E. Scott and J. J. Kodanko, Chem. Commun., 2017, 53, 3673-3676.
- 21 (a) A. A. Khan, K. S. Allemailen, A. Almatroudi, S. A. Almatroodi, M. A. Alsahli and A. H. Rahmani, J. Drug Delivery Sci. Technol., 2021, 61, 102315; (b) B. Rousselle, F. Bouyer, J. Bayardon, M. Laly, F. Ghiringhelli, Y. Rousselin, E. Bodio and R. Malacea-Kabbara, Dalton Trans., 2021, 50, 4880-4889; (c) M. Ali, L. Dondaine, A. Adolle, C. Sampaio, F. Chotard, P. Richard, F. Denat, A. Bettaieb, P. Le Gendre, V. Laurens, C. Goze, C. Paul and E. Bodio, J. Med. Chem., 2015, 58, 4521-4528.
- 22 R. S. Correa, L. M. Bomfim, K. M. Oliveira, D. R. M. Moreira, M. B. P. Soares, J. Ellena, D. P. Bezerra and A. A. Batista, J. Biol. Inorg Chem., 2019, 198, 110751.
- 23 Y. R. Pérez and R. Etchenique, Photochem. Photobiol. Sci., 2019, 18, 208-212.
- 24 S. M. Veronica, M. Alvarez, O. Filevich, R. Etchenique and A. del Campo, Langmuir, 2012, 28, 1217–1221.
- 25 L. Zayat, M. G. Noval, J. Campi, C. I. Calero, D. J. Calvo and R. Etchenique, Chembiochem, 2007, 8, 2035-2038.
- 26 S. K. Lee, M. Kondo, G. Nakamura, M. Okamura and S. Masaoka, Chem. Commun., 2018, 54, 6915-6918.

27 I. M. Dixon, E. Lebon, G. Loustau, P. Sutra, L. Vendier and A. Juris, Dalton Trans., 2008, 5627-5635.

Chemical Science

- 28 E. Lebon, I. M. Dixon, L. Vendier, A. Igau and P. Sutra, Inorg. Chim. Acta, 2007, 360, 1235-1239.
- 29 I. M. Dixon, E. Lebon, P. Sutra and A. Igau, Chem. Soc. Rev., 2009, 38, 1621-1634.
- 30 D. V. Pinnick and B. Durham, *Inorg. Chem.*, 1984, 23, 1440-
- 31 L. Zayat, O. Filevich, L. Baraldo and R. Etchenique, Philos. Trans. R. Soc., A, 2013, 371, 20120330.
- 32 J. D. Knoll, B. A. Albani and C. Turro, Chem. Commun., 2015, **51**, 8777-8780.
- 33 L. M. Loftus, A. Li, K. L. Fillman, P. D. Martin, J. J. Kodanko and C. Turro, J. Am. Chem. Soc., 2017, 139, 18295-18306.
- 34 T. N. Rohrabaugh, Jr., K. A. Collins, C. Xue, J. K. White, J. J. Kodanko and C. Turro, Dalton Trans., 2018, 47, 11851-11858.
- 35 W.-S. Huang, S. Liu, D. Zou, M. Thomas, Y. Wang, T. Zhou, J. Romero, A. Kohlmann, F. Li, J. Qi, L. Cai, T. A. Dwight, Y. Xu, R. Xu, R. Dodd, A. Toms, L. Parillon, X. Lu, R. Anjum, S. Zhang, F. Wang, J. Keats, S. D. Wardwell, Y. Ning, Q. Xu, L. E. Moran, Q. K. Mohemmad, H. G. Jang, T. Clackson, N. I. Narasimhan, V. M. Rivera, X. Zhu, D. Dalgarno and W. C. Shakespeare, J. Med. Chem., 2016, **59**, 4938-4964.
- 36 R. Wang, Y. Chen, X. Zhao, S. Yu, B. Yang, T. Wu, J. Guo, C. Hao, D. Zhao and M. Cheng, Eur. J. Med. Chem., 2019, 183, 111716.
- 37 J. Tu, L. T. Song, H. L. Zhai, J. Wang and X. Y. Zhang, Int. J. Biol. Macromol., 2018, 118, 1149-1156.
- 38 S. Bischoff and M. Kant, *Catal. Today*, 2001, **66**, 183–189.
- 39 A. Riisager, K. M. Eriksen, P. Wasserscheid and R. Fehrmann, Catal. Lett., 2003, 90, 149–153.
- 40 B. A. Harper, D. A. Knight, C. George, S. L. Brandow, W. J. Dressick and C. S. Dalcey, Inorg. Chem., 2003, 42, 516-524.
- 41 B. A. Albani, C. B. Durr and C. Turro, J. Phys. Chem. A, 2013, 117, 13885-13892.
- 42 Z. Assefa and D. M. Stanbury, J. Am. Chem. Soc., 1997, 119, 521-530.
- 43 M. A. Bennett and A. K. Smith, J. Chem. Soc., Dalton Trans., 1974, 233-241.
- 44 A. Alberti, P. Astolfi, P. Carloni, L. Greci, C. Rizzoli and P. Stipa, New J. Chem., 2015, 39, 8964-8970.
- 45 V. V. Pavlishchuk and A. W. Addison, Inorg. Chim. Acta, 2000, **298**, 97-102.
- 46 M. J. Frisch, G. W. Trucks, H. B. Schlegel, G. E. Scuseria, M. A. Robb, J. R. Cheeseman, G. Scalmani, V. Barone, G. A. Petersson, H. Nakatsuji, X. Li, M. Caricato, A. Marenich, J. Bloino, B. G. Janesko, R. Gomperts, B. Mennucci, H. P. Hratchian, J. V. Ortiz, A. F. Izmaylov, J. L. Sonnenberg, D. Williams-Young, F. Ding, F. Lipparini, F. Egidi, J. Goings, B. Peng, A. Petrone, T. Henderson,
 - D. Ranasinghe, V. G. Zakrzewski, J. Gao, N. Rega,
 - G. Zheng, W. Liang, M. Hada, M. Ehara, K. Toyota, R. Fukuda, J. Hasegawa, M. Ishida, T. Nakajima, Y. Honda,
 - Kitao, Nakai, T. Vreven, K. Throssell, H.

- J. A. Montgomery Jr, J. E. Peralta, F. Ogliaro, M. Bearpark, J. J. Heyd, E. Brothers, K. N. Kudin, V. N. Staroverov, T. Keith, R. Kobayahsi, J. Normand, K. Raghavachari, A. Rendell, J. C. Burant, S. S. Iyengar, J. Tomasi, M. Cossi, J. M. Millam, M. Klene, C. Adamo, R. Cammi, J. W. Ochterski, R. L. Martin, K. Morokuma, O. Farkas, J. B. Foresman and D. J. Fox, Gaussian 09, revision E.01. Gaussian, Inc.: Wallingford, CT, 2016.
- 47 D. Andrae, U. Häußermann, M. Dolg, H. Stoll and H. Preuß, Theor. Chim. Acta, 1990, 77, 123-141.
- 48 A. Schäfer, H. Horn and R. Ahlrichs, J. Chem. Phys., 1992, 97, 2571-2577.
- 49 J. P. Perdew, K. Burke and M. Ernzerhof, Phys. Rev. Lett., 1996, 77, 1396.
- 50 J. P. Perdew, K. Burke and M. Ernzerhof, Phys. Rev. Lett., 1996, 77, 3865-3868.
- 51 A. D. Becke, Phys. Rev. A, 1988, 38, 3098-3100.
- 52 C. Lee, W. Yang and R. G. Parr, Phys. Rev. B: Condens. Matter Mater. Phys., 1988, 37, 785-789.
- 53 B. Miehlich, A. Savin, H. Stoll and H. Preuss, Chem. Phys. Lett., 1989, 157, 200-206.
- 54 Chemcraft; Graphical Software for Visualization of Quantum Chemistry Computations. https://www.chemcraftprog.com.
- 55 S. I. Gorelsky and A. B. P. Lever, J. Organomet. Chem., 2001, 635, 187-196.
- 56 S. I. Gorelsky, AOMix: Program for Molecular Orbital Analysis, 2015.
- 57 A. G. Orpen and N. G. Connelly, J. Chem. Soc., Chem. Commun., 1985, 19, 1310-1311.
- 58 D. M. Klassen, Chem. Phys. Lett., 1982, 93, 383-386.
- 59 M. Mitoraj and A. Michalak, Organometallics, 2007, 26, 6576-6580.
- 60 B. A. Albani, B. Peña, K. R. Dunbar and C. Turro, Photochem. Photobiol. Sci., 2014, 13, 272-280.
- 61 P. Bonneson, J. L. Walsh, W. T. Pennington, A. W. Cordes and B. Durham, Inorg. Chem., 1983, 22, 1761-1765.
- 62 A. Juris, S. Campagna, V. Balzani, G. Gremaud and A. von Zelewsky, Inorg. Chem., 1988, 27, 3652-3655.
- 63 L. M. Loftus, K. F. Al-Afyouni, T. N. Rohrabaugh Jr, J. C. Gallucci, C. E. Moore, J. J. Rack and C. Turro, J. Phys. Chem. C, 2019, 123, 10291-10299.
- 64 L. M. Loftus, K. F. Al-Afyouni and C. Turro, Chem. Eur. J., 2018, 24, 11550-11553.
- 65 E. Wachter, D. K. Heidary, B. S. Howerton, S. Parkin and E. C. Glazer, Chem. Commun., 2012, 48, 9649-9651.
- 66 E. Baranoff, J.-P. Collin, J. Furusho, Y. Furusho, A.-C. Laemmel and J.-P. Sauvage, Inorg. Chem., 2002, 41, 1215-1222.
- 67 J. V. Caspar and T. J. Meyer, Inorg. Chem., 1983, 22, 2444-
- 68 B. Durham, J. V. Caspar, J. K. Nagle and T. J. Meyer, J. Am. Chem. Soc., 1982, 104, 4803-4810.
- 69 B. Durham, J. L. Walsh, C. L. Carter and T. J. Meyer, *Inorg.* Chem., 1980, 19, 860-865.
- 70 G. H. Allen, R. P. White, D. P. Rillema and T. J. Meyer, J. Am. Chem. Soc., 1984, 106, 2613-2620.

Edge Article

- 71 J. D. Knoll, B. A. Albani, C. B. Durr and C. Turro, J. Phys. Chem. A, 2014, 118, 10603-10610.
- 72 S. Bonnet, J. P. Collin, J. P. Sauvage and E. Schofield, Inorg. Chem., 2004, 43, 8346-8354.
- 73 A.-C. Laemmel, J.-P. Collin and J.-P. Sauvage, Eur. J. Inorg. Chem., 1999, 383-386.
- 74 B. S. Howerton, D. K. Heidary and E. C. Glazer, J. Am. Chem. Soc., 2012, 134, 8324-8327.
- 75 M. H. Al-Afyouni, T. N. Rohrabaugh, K. F. Al-Afyouni and C. Turro, Chem. Sci., 2018, 9, 6711-6720.
- 76 M. Abrahamsson, M. Jäger, R. J. Kumar, T. Österman, Persson, H. C. Becker, O. Johansson L. Hammarström, J. Am. Chem. Soc., 2008, 130, 15533-15542.
- 77 J. Romanova, Y. Sadik, M. R. Ranga Prabhath, J. D. Carey and P. D. Jarowski, J. Phys. Chem. C, 2017, 121, 2333-2343.
- 78 E. Galardon, P. Le Maux, L. Toupet and G. Simonneaux, Organometallics, 1998, 17, 565-569.
- 79 A. C. H. Da Silva, J. L. F. Da Silva and D. W. Franco, Dalton Trans., 2016, 45, 4907-4915.

- 80 S. D. Ramalho, R. Sharma, J. K. White, N. Aggarwal, A. Chalasani, M. Sameni, K. Moin, P. C. Vieira, C. Turro, J. J. Kodanko and B. F. Sloane, PLoS One, 2015, 10, e0142527/1-e0142527/17.
- 81 N. P. Toupin, S. Nadella, S. J. Steinke, C. Turro and J. J. Kodanko, Inorg. Chem., 2020, 59, 3919-3933.
- 82 A. P. Languist, S. Gupta, M. Al-Afyouni, J. J. Kodanko and C. Turro, Chem. Sci., 2021, 12, 12056-12067.
- 83 B. A. Albani, B. Peña, N. A. Leed, N. A. B. G. de Paula, C. Pavani, M. S. Baptista, K. R. Dunbar and C. Turro, J. Am. Chem. Soc., 2014, 136, 17095-17101.
- 84 H. Scheffler, Y. You and I. Ott, Polyhedron, 2010, 29, 66-69.
- 85 V. Gandin, A. P. Frenandes, M. P. Rigobello, B. Dani, F. Sorrentino, F. Tisato, A. Björnstedt, A. Bindoli, A. Sturaro, R. Rella and C. Marzano, Biochem. Pharmacol., 2010, 79, 90-101.
- 86 C. Icsel, V. T. Yilmaz, B. Cevatemre, M. Avgun and E. Ulukaya, J. Biol. Inorg Chem., 2020, 25, 75-87.